Contribution of the Orbiting Carbon Observatory to the estimation of CO 2 sources and sinks: Theoretical study in a variational data assimilation framework

Frederic Chevallier, Francois-Marie Breon, Peter Rayner

Contribution of the Orbiting Carbon Observatory to the estimation of CO_2 sources and sinks: Theoretical study in a variational data assimilation framework

Frédéric Chevallier,[1] François-Marie Bréon,[1] and Peter J. Rayner[1]

Received 6 April 2006; revised 9 November 2006; accepted 14 December 2006; published 8 May 2007.

[1] NASA's Orbiting Carbon Observatory will monitor the atmospheric concentrations of carbon dioxide (CO_2) along the satellite subtrack over the sunlit hemisphere of the Earth for more than 2 years, starting in late 2008. This paper demonstrates the application of a variational Bayesian formalism to retrieve fluxes at high spatial and temporal resolution from the satellite retrievals. We use a randomization approach to estimate the posterior error statistics of the calculated fluxes. Given our prior information about the fluxes (with error standard deviations about 0.4 g C m^{-2} d^{-1} over ocean and 4 g C m^{-2} d^{-1} over vegetated areas) and our observation characteristics (with error standard deviations about 2 ppm), we show error reductions of up to about 40% at weekly scale for a grid point of the transport model. We simulate the impact of undetected biases by perturbing the observations and show that regional biases of a few tenths of a part per million in column-averaged CO_2 can bias the inverted yearly subcontinental fluxes by a few tenths of a gigaton of carbon, which is larger than the uncertainty on the anthropogenic carbon fluxes but smaller than that of natural fluxes over most vegetated areas.

Citation: Chevallier, F., F.-M. Bréon, and P. J. Rayner (2007), Contribution of the Orbiting Carbon Observatory to the estimation of CO_2 sources and sinks: Theoretical study in a variational data assimilation framework, *J. Geophys. Res.*, *112*, D09307, doi:10.1029/2006JD007375.

1. Introduction

[2] The carbon cycle in the Earth system results from the exchange of huge amounts of carbon compounds between the atmosphere, the ocean, the biosphere, and the fossil reservoirs (several tens of gigatons of carbon per year). Since the cycle is nearly stationary on a yearly timescale, the annual global net flux at the interface between the atmosphere and the Earth is close to zero, with a relatively small gain for the atmosphere (about 3 Gt C per year, mainly of CO_2). This slight imbalance feeds back on another near-balanced budget, that of the energy exchange between the Earth system and outer space, via radiation processes. The importance of the topic has triggered numerous efforts to better quantify the carbon surface fluxes at all spatial scales.

[3] The Orbiting Carbon Observatory (OCO) [*Crisp et al.*, 2004] has been chosen by NASA to remotely sense atmospheric CO_2 from space and is planned for launch in late 2008. From its high-resolution spectroscopic measurements of reflected sunlight, this instrument will provide the data needed to retrieve the column-averaged dry air mole fraction of CO_2, denoted X_{CO2}, over the sunlit part of the globe. The number of cloud-free soundings and precision per sounding will vary with latitude, cloud cover, aerosol optical depth, and other factors, but the minimum requirement of the mission is to achieve X_{CO2} precision of 1 ppm for monthly averages over regional (1000×1000 km^2) spatial scales. Building on the experience using in situ gas concentration measurements [e.g., *Gurney et al.*, 2002], inverse methods will be applied to quantify the CO_2 surface sources and sinks from the OCO retrievals. The usefulness of satellite data for such a task has been demonstrated from simulations at relatively low spatial and temporal resolutions [*Rayner and O'Brien*, 2001; *Pak and Prather*, 2001; *Houweling et al.*, 2004]. Higher resolutions are being introduced thanks to a variational formulation of the Bayesian inversion problem [*Chevallier et al.*, 2005b; *Rödenbeck*, 2005]. However, the inversion of existing satellite CO_2 products has not been successful so far most likely because of the existence of biases both in the observations and in the transport models [*Chevallier et al.*, 2005a, 2005b; *Houweling et al.*, 2005]. Furthermore, some of these observations are restricted to the upper troposphere, which is only remotely connected to the surface. In the light of these recent developments, this paper evaluates the usefulness of the forthcoming OCO measurements for characterizing surface fluxes, based on a series of observing system simulation experiments. The design of the experiments allows us to estimate some diagnostic quantities, like the degrees of

[1]Laboratoire des Sciences du Climat et de l'Environnement, Institut Pierre-Simon Laplace, Commissariat àl'Energie Atomique, Centre National de la Recherche Scientifique, Universitéde Versailles Saint-Quentin-en-Yvelines, Gif-sur-Yvette, France.

0148-0227/07/2006JD007375

freedom for signal or the error reduction, that are usually difficult to obtain for high-dimensional problems. To summarize, our study approaches two distinct scientific problems: a methodological issue regarding variational systems in general, and the relevance of OCO to improve our knowledge about the carbon cycle. Our method and our data are described in the following section. Section 3 presents the results, which are discussed in section 4.

2. Method and Data

[4] The steps in our observing system simulation experiments (OSSE) can be described as follows:

[5] 1. Use a climatology of surface fluxes as boundary conditions to a transport model and generate a set of pseudo observations.

[6] 2. Perturb the pseudo-observations consistently with assumed observation error statistics.

[7] 3. Perturb the surface flux climatology consistently with assumed error statistics.

[8] 4. Perform a Bayesian inversion using the perturbed pseudo-observations as data and the perturbed climatology as the prior field.

[9] 5. Compare the estimate of the inversion to the flux climatology to get the errors in the estimate.

[10] The ingredients of this procedure are detailed in the next subsections.

2.1. Inversion Scheme

[11] Bayesian inference describes how observations $\mathbf{y}$ transform our knowledge about any related variables $\mathbf{x}$. It has been particularly useful in numerous fields, although it is often difficult to define the required error statistics on the prior information and on the observations. It is at the root of CO_2 surface flux estimations at the global scale [e.g., *Enting et al.*, 1995; *Gurney et al.*, 2002; *Enting*, 2002]. The main developments of the method for CO_2 since its introduction in the 90 s are twofold. First the realism of its ingredients has been improved: the transport model H which simulates the atmospheric concentrations $\mathbf{y}$ from the surface fluxes $\mathbf{x}$, and, to a lesser extent, the error covariance matrices $\mathbf{B}$ and $\mathbf{R}$ that describe the error statistics, assumed to be Gaussian and bias free, for $\mathbf{x}$ and $\mathbf{y}$ respectively. Second, the spatial and temporal resolutions of $\mathbf{x}$ and $\mathbf{y}$ have been dramatically increased, thanks to the evolution of computer power and, only recently, to the implementation of a variational formulation to the optimization problem [*Chevallier et al.*, 2005b; *Rödenbeck*, 2005; *Baker et al.*, 2006], as is done in numerical weather prediction (NWP).

[12] In this study, the control variables $\mathbf{x}$ are the CO_2 surface fluxes either at daytime or at nighttime, at each point of a $3.75^\circ \times 2.5^\circ$ (longitude-latitude) grid every 8 days. Daytime and nighttime fluxes are defined separately to account for the diurnal cycle of the biospheric fluxes. The motivation for the 8-day resolution is given in the coming section 2.3 from considerations about the prior errors. In the simulations presented here, fluxes within any of the 8-day periods are interpolated in time from the control variables. The 3D carbon field at the start of the assimilation window is also included in the vector $\mathbf{x}$ but the length of the temporal window (one year) makes it play a minor role. The general circulation model of the Laboratoire de Météorologie Dynamique (LMDZ) [*Sadourny and Laval*, 1984; *Hourdin and Armengaud*, 1999], nudged to NWP winds, is our H operator. LMDZ is used here with 19 levels in the vertical and the same horizontal resolution as the surface fluxes.

[13] The concentrations $\mathbf{y}$ are here individual OCO retrievals of X_{CO2}, binned per orbit at the $3.75^\circ \times 2.5^\circ$ model resolution. As mentioned in the introduction, they are distributed in cloud-free sunlit areas only and therefore constrain the control variables in a complicated way. For instance, a midday X_{CO2} observation is not influenced by the surface fluxes later in the day but may integrate significant information about the fluxes from the night before.

[14] The variational inversion system of *Chevallier et al.* [2005b] allows us to find the optimal fluxes $\mathbf{x}_a$ that fit both the observations $\mathbf{y}$ with their specified error statistics $\mathbf{R}$ and the prior fluxes $\mathbf{x}_b$ with their specified error statistics $\mathbf{B}$, by iteratively minimizing the cost function J defined by

$$J(\mathbf{x}) = (\mathbf{x}-\mathbf{x_b})^{\mathrm{T}}\mathbf{B}^{-1}(\mathbf{x}-\mathbf{x_b}) + (H(\mathbf{x})-\mathbf{y})^{\mathrm{T}}\mathbf{R}^{-1}(H(\mathbf{x})-\mathbf{y}) \quad (1)$$

Our notation follows *Ide et al.* [1997]. One may notice in equation (1) that J accounts for random errors only. Systematic errors in the prior or in the observations are supposed to have been removed before the minimization.

[15] The number of iterations needed for the minimization of $J(\mathbf{x})$ to reach convergence depends not only on the degree of nonlinearity and on the conditioning of the minimization problem, but also on the minimization strategy. The efficiency of the minimization algorithm is particularly crucial when the computational cost of each iteration is high. In our case, a single iteration using 1 year's worth of data takes about 7 CPU hours when using a 64-bit processor at 2.6 GHz. This high computation burden is explained by the necessity of running the transport model successively in forward mode (to compute $J(\mathbf{x})$) and in adjoint mode (to compute the gradient of $J(\mathbf{x})$) over the whole period at each iteration. Our minimization strategy follows the ''inner loop/outer loop'' approach developed at the European Centre for Medium-Range Weather Forecasts (ECMWF) where operational constraints impose a stringent limitation to the number of iterations for the NWP analyses. As initially described by *Courtier et al.* [1994], the minimization is decomposed into a succession of minimizations for which the observation operator is linearized around the corresponding first guess (using a first-order Taylor expansion). The updates of the linearization constitute the outer loop of this system. The overall convergence of such an ''inner loop/outer loop'' approach depends on the validity of the tangent-linear hypothesis for the size of analysis increments considered [*Trémolet*, 2005]. Note that the transport of a passive tracer, like CO_2, which is a linear process, becomes nonlinear in a numerical model, given the need of the model to prevent unrealistic growth of the gradients while at the same time not being overly diffusive [e.g., *Hourdin and Armengaud*, 1999]. However, the use of a linear model in the inner loop makes the cost function quadratic and allows one to use efficient algorithms like the conjugate gradient methods, as is done here. Conjugate-gradient methods require fewer iterations to converge if the Hessian (matrix of second derivatives J'') of J has a lower

condition number [e.g., *Andersson et al.*, 2000]. Preconditioning techniques reduce the condition number of J'' by an appropriate change of variable. The perfect preconditioner is the change to $\mathbf{z} = (J_x'')^{-1/2}\,\mathbf{x}$, because it makes all the eigenvalues of the preconditioned Hessian J_z'' equal to one and reduces the minimization to a single iteration when using steepest descent or conjugate gradient methods. To draw near to this ideal case, *Courtier et al.* [1994] estimate J_x'' on the basis of a randomized estimate of the covariance matrix of J_x' (the derivative of J with respect to x), while *Fisher and Courtier* [1995] use the Lanczos algorithm to obtain the leading eigenvectors of J_x''. In our case the preconditioning with respect to the prior only, as suggested by *Lorenc* [1988], was found more practical despite its lesser efficiency: $\mathbf{z} = \mathbf{B}^{-1/2}\,(\mathbf{x} - \mathbf{x_b})$ is our minimization control variable rather than $\mathbf{x}$. Note that this change of variable is also used at ECMWF in the first minimization.

[16] The configuration that we have selected is a two-iteration outer loop. Ten iterations are performed in the first inner loop minimization and 40 in the second. This setup was chosen empirically after several tests. It provides numerically stable results at a reasonable computational cost.

2.2. Observations

[17] The atmospheric CO_2 fields used to simulate OCO X_{CO2} data in the present study have been calculated from a climatology of carbon fluxes $\mathbf{x}_{\text{clim}}$ used as the boundary condition for LMDZ. $\mathbf{x}_{\text{clim}}$ is considered to be the truth for the present theoretical study.

[18] The climatology includes three components. First, fossil fuel CO_2 emissions are defined from the EDGAR 3.0 emission database [*Olivier et al.*, 1996]. Second, air-sea CO_2 exchange is prescribed by *Takahashi et al.* [2002] with a sink of 1.8 Gt C per year. Last, the biosphere-atmosphere exchange of CO_2 is estimated by the Terrestrial Uptake and Release of Carbon (TURC) model [*Lafont et al.*, 2002], which is annually balanced. The daily fluxes calculated by TURC have been redistributed throughout the day to account for the diurnal cycle of the fluxes resulting from the photosynthetic activity (M. Heimann, personal communication, 2003). The CO_2 concentrations at the initial time step of the LMDZ simulation are defined from a former simulation using fluxes optimized through the inversion of monthly surface in situ observations [*Bousquet et al.*, 2000].

[19] OCO will fly in the A train with a 705 km Sun-synchronous polar orbit that provides global sampling on a 16-day (233 orbits) repeat cycle with a 1318 local standard time equator crossing [*Crisp et al.*, 2004]. In these simulations, we assume that OCO is in the glint observing mode, where the instrument boresight is pointed off nadir at the specular reflection point. This mode increases the measurement signal to noise over water bodies and provides useful data over both land and ocean. OCO will continuously collect 12 to 24 soundings per second as the satellite moves from pole to pole at 6.8 km per second along its near-polar, Sun-synchronous orbit track. It therefore collects 490 to 980 samples each time it traverses a $3.75^\circ \times 2.5^\circ$ (longitude-latitude) LMDZ grid cell, and each grid cell is traversed two or three times during each 16-day repeat cycle. The sounding foot print size varies from less than 3 km^3 when observing the local nadir, to greater than 25 km^3 at the most extreme viewing angles. Note that the OCO instrument also has a nadir sampling mode, which is believed to be more favorable over land, but less favorable over ocean. The sampling of both modes is rather similar. Simulated X_{CO2} have been individually sampled along the OCO orbit track at the glint location. Since only X_{CO2} retrievals in clear sky conditions provide direct constraints on the surface fluxes, these samples were filtered for clouds. The sampling accounts for a climatological cloud cover [*Rossow et al.*, 1996] as well as for cloud cover spatial correlation statistics [*Bréon et al.*, 2005]. To compute X_{CO2} from the vertical profile of CO_2 concentrations, a uniform weighting function was used (i.e., the relative contribution of a CO_2 molecule does not depend on its pressure level).

[20] The sampled X_{CO2} have been perturbed with the specified observation error statistics $\mathbf{R}$ following:

$$\mathbf{y} = \mathbf{y}_{\text{clim}} + \mathbf{V}^{\mathrm{T}}\mathbf{v}^{1/2}\mathbf{p} \tag{2}$$

with $\mathbf{y}_{\text{clim}} = H(\mathbf{x}_{\text{clim}})$ the simulated X_{CO2}. $\mathbf{V}$ and $\mathbf{v}$ are the eigenvector and eigenvalue matrices of the principal component analysis of $\mathbf{R}$, so that $\mathbf{R} = \mathbf{V}^{\mathrm{T}}\,\mathbf{v}\,\mathbf{V}$. Vector $\mathbf{p}$ is a vector of size the number of observations, which is a realization of random variables with standard normal distributions.

[21] In equation (1), the observation error is defined with respect to the measurement equivalent given by the transport model. Therefore it includes the measurement error, the representativeness error (caused by differences in temporal and spatial resolutions between the observations and the model) and the transport model error. The simulations presented by *Crisp et al.* [2004] indicated random measurement errors between 0.8 and 1.7 ppm for retrievals from individual OCO X_{CO2} soundings. Representativeness and model errors are difficult to quantify but are usually considered to be of the order of 1 ppm for most surface stations [*Rödenbeck et al.*, 2003]. For simplicity we have assumed the total observation error standard deviation to be 2 ppm for all of our data. Following the usual approximation, correlations between the errors of different retrievals (in particular between measurements for each adjacent along-track location, 2.5° apart) are neglected so that equation (2) reduces to

$$\mathbf{y} = \mathbf{y}_{\text{clim}} + \mathbf{v}^{1/2}\mathbf{p} \tag{3}$$

2.3. Prior Information

[22] The prior information $\mathbf{x}_{\mathrm{b}}$ is also specified to be consistent with the above-described "true" fluxes $\mathbf{x}_{\text{clim}}$ and with their specified error matrix $\mathbf{B}$:

$$\mathbf{x}_{\mathrm{b}} = \mathbf{x}_{\text{clim}} + \mathbf{W}^{\mathrm{T}}\mathbf{w}^{1/2}\mathbf{q} \tag{4}$$

where $\mathbf{q}$ is a vector of size the dimension of $\mathbf{x}_{\mathrm{b}}$, which is a realization of random variables with standard normal distributions. $\mathbf{W}$ and $\mathbf{w}$ are the eigenvector and eigenvalue matrices of the principal component analysis of $\mathbf{B}$, so that $\mathbf{B} = \mathbf{W}^{\mathrm{T}}\,\mathbf{w}\,\mathbf{W}$. The covariance matrix $\mathbf{B}$ is defined below.

[23] The correlations of $\mathbf{B}$ are assigned from basic considerations about the origin of errors in the prior fluxes.

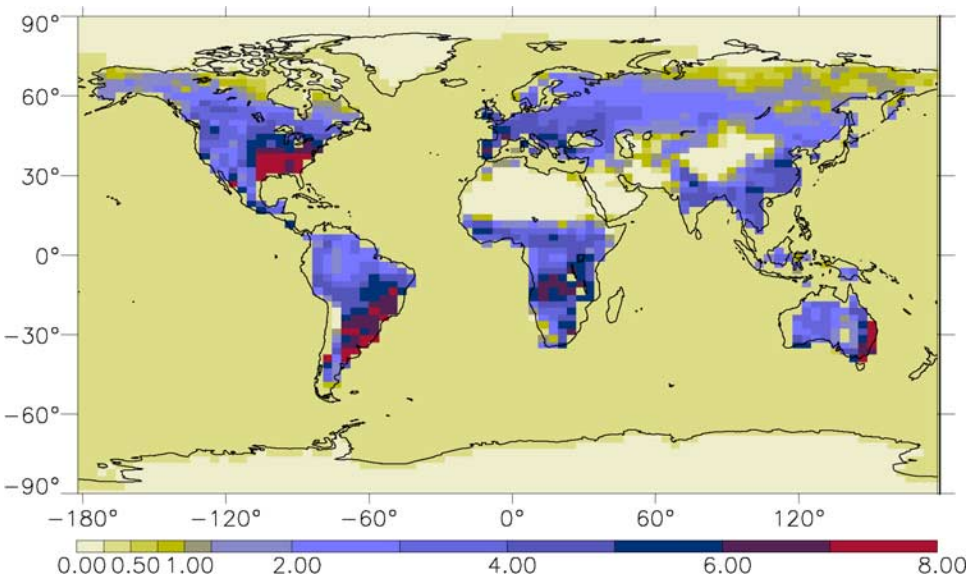

Figure 1. Standard deviation of the prior errors, in g C m^{-2} d^{-1}.

Since the processes involved are different for land and for sea, the errors are supposed to be uncorrelated between these two geotypes. *Chevallier et al.* [2006] suggested that current prior errors for vegetation fluxes have significant temporal autocorrelations (i.e., larger than 0.5) within about a fortnight. For the sake of simplicity, land and sea fluxes are defined here with an 8-day temporal resolution and with zero error temporal correlations from one 8-day period to the next and between daytime and nighttime. Spatial correlations are specified as a function of distance as, e.g., in the study by *Rödenbeck et al.* [2003]. Correlation *e*-folding lengths are set to 500 km over land, which implies error patterns of about the size of France. This value is about the smallest possible given the scale of the transport model (415 × 275 km^2 at the equator) and is motivated by the large spatial variability of biospheric carbon fluxes that should tend to decorrelate errors [*Chevallier et al.*, 2006]. Spatial scales are larger over oceans and an *e*-folding length of 1000 km over the ocean was chosen. It specifies the size of coherent error patterns to be about that of the Bay of Bengal. The square root of the sum of the error covariances for the individual fluxes was set to 0.8 and 2.0 Gt C per year for ocean and land respectively which is consistent with our current uncertainty about the global carbon budget [*Intergovernmental Panel on Climate Change*, 2001]. The errors were spread in space proportionally to grid size over ocean and to the annual mean heterotrophic respiration flux modeled by TURC over land. There is no seasonality in these errors. The resulting error standard deviations are shown in Figure 1. Standard deviations of the errors of the CO_2 concentrations at the initial time step of the LMDZ simulation are set to 1% in each grid box, with unity vertical correlations and the same spatial correlations than the fluxes. The results presented here are only marginally affected by the formulation of the errors of the initial state, given the length of the temporal window considered (1 year).

[24] It is of interest to mention that the inversion of **B** in equation (1) and its eigenvalue decomposition in (4) are facilitated despite its large dimension because **B** is block diagonal (zero temporal correlations). Still, temporal correlations can be easily introduced as long as the matrix remains sparse, for instance using its principal components. Once the eigenvalue decomposition is available, the minimization control variable **z** (see section 2.1) can be computed in a simple way by expressing it as

$$\mathbf{z} = \mathbf{W}^{\mathbf{T}}\mathbf{w}^{-1/2}(\mathbf{x} - \mathbf{x_b}) \tag{5}$$

2.4. Inversions

[25] Five inversions have been performed. Each of them covers 12 months, using meteorological conditions valid for year 2003. They only differ from each other by the vectors of perturbations **p** and **q** (that have standard normal distribution, as explained in section 2.2). The simulated OCO orbit and cloud cover give 243,689 independent observations at the horizontal resolution of the LMDZ transport model (the cloud screening removed 30% of the original data). By comparison, the dimension of the control vector is about 631,000 (i.e., twice-a-day grid point fluxes every 8 days during 1 year). OCO will actually provide hundreds of observations within a model grid box in most cases. However, the existence of large correlations among the measurement errors and of the representativeness errors between these makes it difficult to assimilate them all individually. Therefore each one of the 243,689 observations may be considered either as an average value of the measurements along the corresponding portion of the satellite orbit, or as a sample of these. Depending on the actual value of the measurement error correlations within a model grid box, this subsampling may underestimate the strength of the constraint available from the full OCO measurement data set.

3. Results

[26] A number of useful diagnostics about the inversion system are directly available as by-products of the inver-

sions. This is particularly the case when the system satisfies consistency, such as ours, as ensured by (2) and (4). The diagnostics are detailed in the following.

3.1. Linearity of the Transport Model

[27] The validity of the tangent-linear hypothesis used in the minimization can be evaluated in different ways [e.g., *Janisková et al.*, 2002]. Here, the impact of nonlinearities in the transport model can be simply noticed when studying the distribution of the variable $\mathbf{a} = H(\mathbf{x}_b) - H(\mathbf{x}_{clim})$. From equation (4), **a** should be unbiased in the case of a linear operator since $\mathbf{W}^T \mathbf{w}^{1/2}$ **q** is unbiased by definition. Here **a** is actually unbiased only south of 50°N. Limiters of the tracer slopes in the advection scheme [*Hourdin and Armengaud*, 1999] bias **a** by up to 0.8 ppm around the North Pole (not shown). Indeed they slightly slow down the poleward transport in the presence of the large surface gradients introduced by $\mathbf{W}^T \mathbf{w}^{1/2}$ **q** between the vegetated areas of the Northern hemisphere and the polar cap, to preserve the monotonicity of the scheme.

[28] The comparison between the reduction of the magnitude in the gradient J_z' of the quadratic cost function J and the reduction for that of the real (nonlinear) function provides another evaluation of the tangent-linear hypothesis. In our case, the first ten iterations reduce the gradient of the quadratic J by a factor between ten and twenty in the five inversions performed. The gradient reduction for the real J is about the same. However, at the end of the second inner loop (see section 2.1), significant differences are noticed between the two versions of the gradient. The gradient of the quadratic J is reduced by about a 20-fold factor when the norm of the real J_z' is reduced by a factor about 4 only. This feature justifies not adding more iterations in the second inner loop, but a third inner loop may further reduce the discrepancy, since it generates smaller increments than the second one if the inner loop/outer loop system converges (see section 2.1).

3.2. Condition Number of the Minimization

[29] As discussed in section 2.1, the rate of convergence of the minimization is largely determined by the condition number of J_z''. Further to our change of variable $\mathbf{z} = \mathbf{B}^{-1/2}\,\mathbf{x}$, the smallest eigenvalue of J_z'' equals 1 and its condition number is its leading eigenvalue. As can be seen from equation (1), J_z'' does not depend on the values of the observations nor on the prior, but only on the spatiotemporal structure of their error statistics and the observation operator. Its leading eigenvalues are provided by the Lanczos algorithm as a by-product of the conjugate-gradient minimization [*Fisher*, 1998]. In our case, the condition number is about 41,600. By comparison, the condition number for the ECMWF weather analyses is about 3000 when using the same conditioning as here [*Andersson et al.*, 2000]. Our relatively large condition numbers indicate that the observations are much more accurate than the prior or that the density of the observations is large compared to the surface flux error patterns [*Andersson et al.*, 2000]. Both explanations may be valid for OCO.

3.3. Number of Iterations

[30] The value of the cost function at the end of the minimization provides an interesting diagnostic of the convergence. Indeed, for a consistent system and given a realization of the observations **y**, the cost function at the minimum $J(\mathbf{x_a})$ is chi square distributed with expectation and variance equal to the number of observations N [e.g., *Talagrand*, 1998; *Ménard et al.*, 2000]. Our idealized system is consistent by construction and $J(\mathbf{x})$ converges toward N indeed, starting from about 330,000 and reaching about 244,000, given about 243,689 observations. This result justifies nonpursuing the minimization after our second inner loop.

3.4. Degrees of Freedom for Signal

[31] The quantity $J_b(\mathbf{x_a}) = (\mathbf{x_a} - \mathbf{x_b})^T\,\mathbf{B}^{-1}\,(\mathbf{x_a} - \mathbf{x_b})$ which is used for the computation of $J(\mathbf{x_a})$ reflects the number of degrees of freedom for signal (DFS) [e.g., *Rodgers*, 2000]. The DFS describes the number of independent pieces of information that the observations provide, given the prior information. $J_b(\mathbf{x_a})$ is actually a small fraction of $J(\mathbf{x_a})$ in our case. Even though the latter is rather stable after the second inner loop minimization, the former still increases from one iteration to the next and its value should be considered as a lower bound. We get numbers about 6000, which indicates that more than 6000 independent quantities about the fluxes can be measured from a year of OCO data. Unsurprisingly, the 244,000 OCO X_{CO2} measurements yield significantly more surface flux information than the 347,000 TOVS measurements studied by *Chevallier et al.* [2005b] that were less accurate and restricted to the tropical upper troposphere (they had 340 DFS).

3.5. Error Reduction

[32] The statistical characteristics of the analysis error are another very useful quantity. They will be one of the key metrics to evaluate the usefulness of the X_{CO2} data product. Given unbiased Gaussian error statistics for the observations and the prior, and a linear transport model, the analysis errors are also unbiased and Gaussian, and can be fully described by a covariance matrix **A**. The analysis error covariance matrix **A** can be written in various analytical forms [e.g., *Rodgers*, 2000]. They are exact as long as the error statistics of the observations and of the prior are correctly described. All of these expressions require the inversion of matrices that are too large to be feasible for the current study. Instead of using these given exact expressions, we take advantage here of the fact that the statistics of the analysis errors are the statistics of the differences between $\mathbf{x}_a$ and our "truth" $\mathbf{x}_{clim}$. Such an a posteriori estimation is all the more reliable since the statistical sample is large. The high computational cost of an inversion prevents the accumulation of many inversion results, but each 1-year inversion inherently contains 45 global maps of 8-day fluxes. The five inversions thus generate an ensemble of 225 maps that allow us to estimate the annual mean variance of the analysis errors of the 8-day fluxes. Note that temporal correlations are absent in our prior errors and in our observation errors, but are induced in the analysis by the atmospheric transport. Therefore the number of truly independent realizations of the 8-day fluxes is smaller. To estimate the errors on the monthly fluxes, 60 realizations are available.

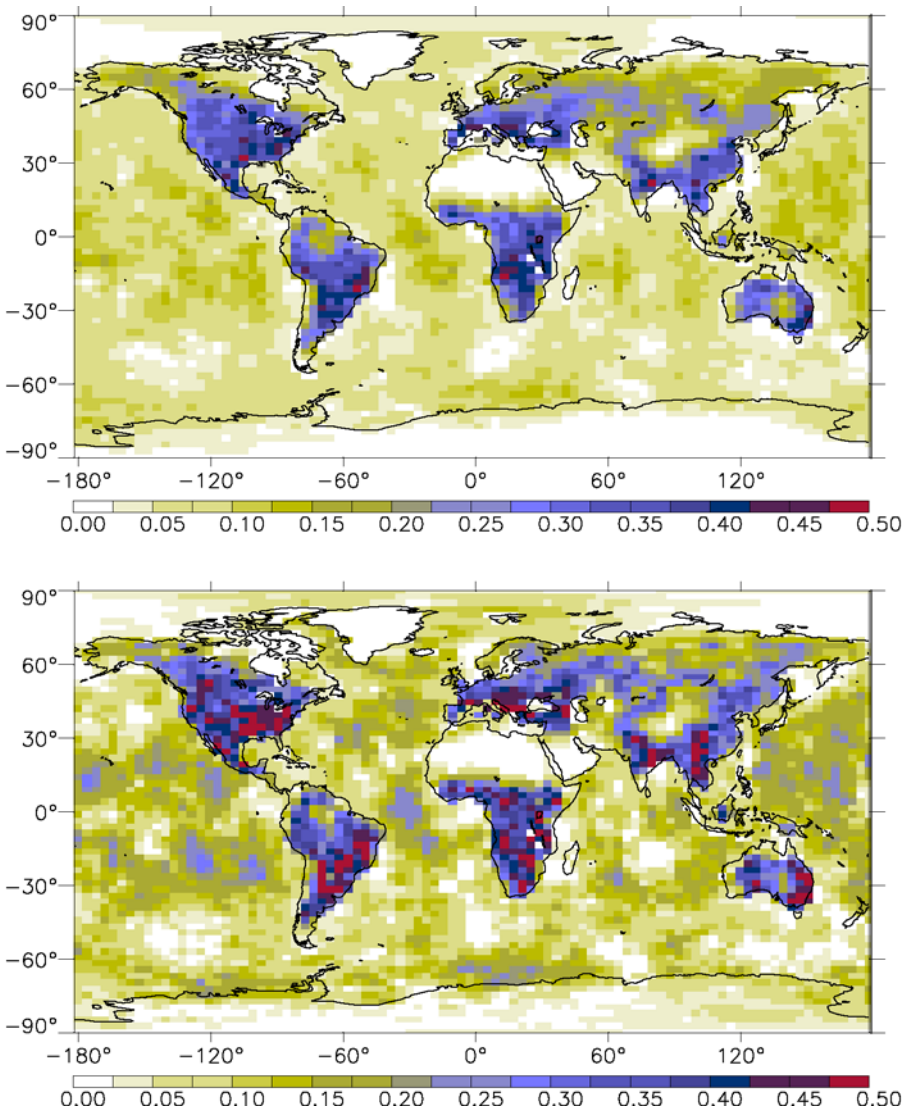

Figure 2. Fractional error reduction of (top) the 8-day mean and (bottom) the monthly mean grid point CO_2 surface fluxes. The error reduction is defined as $(1 - \sigma_a/\sigma_b)$, where σ_a is the posterior error standard deviation and σ_b is the prior error standard deviation. The map of σ_b for the 8-day mean fluxes is shown in Figure 1.

[33] The existence of spatial and temporal correlations in the analyzed flux increments makes the error reduction scale-dependent. Positive correlations between the errors of the individual fluxes (i.e., large increments in space or time) tend to increase the errors of the aggregated fluxes. Negative correlations (i.e., dipoles) have the opposite effect. Figure 2 displays the global map of the estimated uncertainty reduction achieved by the analysis for 8-day fluxes and monthly fluxes. In both cases, daytime and nighttime fluxes have been aggregated together. By definition, these error reductions are relative to our prior errors (section 2.3) and would vary with other error characteristics. The map for 8-day (monthly) fluxes displays error reduction of 0–15% (0–25%) for fluxes over oceans and over boreal forests, and of about 15–45% (20–50%) over other vegetated areas. The patterns are robust with respect to the individual realizations. For instance, using any 2 years only, out of the five available, gives the same patterns. They rather reproduce the spatial variations of the background errors (Figure 1), with larger reductions where the prior errors are larger, i.e., over the vegetated areas, and smaller reductions where the prior errors are negligible, i.e., over the polar caps and over the deserts. Over the oceans, where our background errors are the same everywhere and are smaller than over vegetated land, the relatively small error reduction is controlled by the meteorology and by the observation location, which are the same in the five simulations. The error reduction is smaller when separating daytime and nighttime fluxes (not shown). This feature shows the existence of large negative correlations between the two types of fluxes, or, in other words, confirms the ambiguity of X_{CO2} information with respect to surface fluxes at subdaily timescales.

[34] The impact of spatial aggregation is illustrated by aggregating the fluxes within the 11 land and 11 ocean regions defined in phase 3 of the Atmospheric Tracer

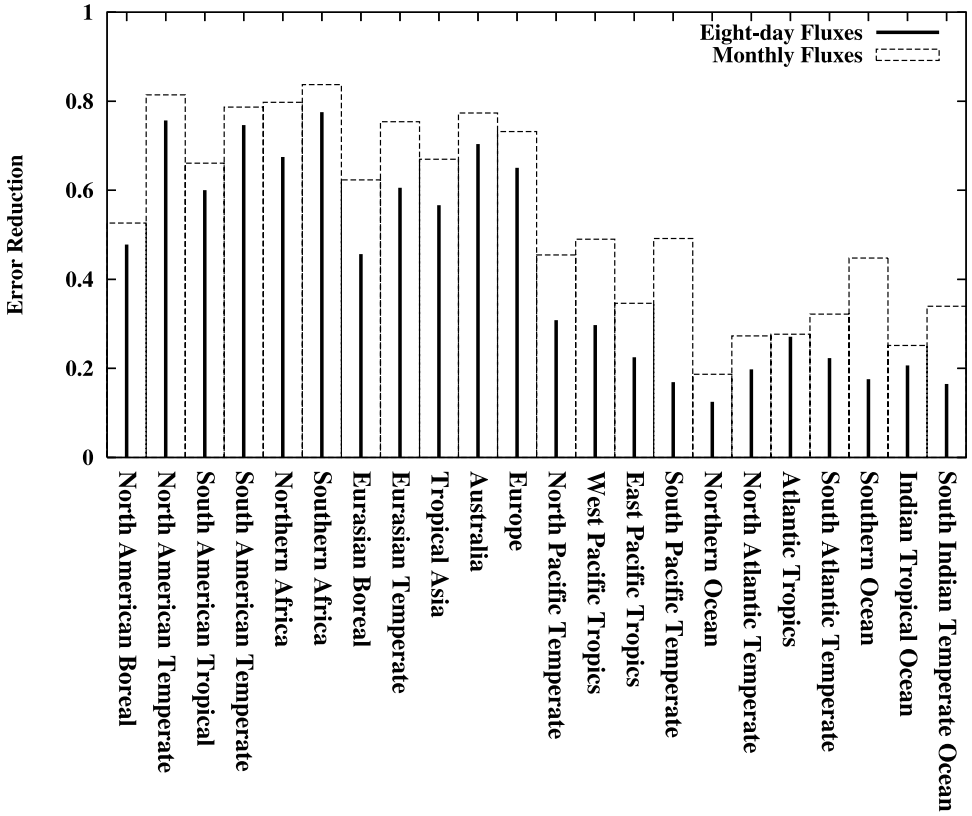

Figure 3. Fractional error reduction of the CO_2 surface fluxes over the 22 TransCom-3 regions. Results for monthly and for 8-day fluxes are shown. As in Figure 2, the error reduction is defined as $(1 - \sigma_a/\sigma_b)$, where σ_a is the posterior error standard deviation and σ_b is the prior error standard deviation.

Transport Model Intercomparison Project (TransCom3) [*Gurney et al.*, 2002]. Together with the ice caps (23rd region with negligible fluxes and uncertainties), they cover the globe entirely. Figure 3 presents the fractional change in flux uncertainty for the 22 regions. It emphasizes the better constraint of the monthly fluxes versus the 8-day ones, in particular over oceans. One may also notice that the TransCom3-scale error reduction is larger than at the grid point scale, in particular over land where the reduction rises to 50–80%. Indeed the ambiguity of the X_{CO2} information with respect to the spatial location of the fluxes translates into negative spatial error correlations in the analyzed fluxes, attenuated by our specified error correlation lengths (smaller over land than over oceans, section 2.3).

3.6. Tolerance to Observational Biases

[35] The error reduction estimated in the previous section is strictly theoretical. In practice, inadequate specifications of the error statistics introduce inconsistencies and prevent the inversions from converging on optimal fluxes. The detrimental impact of undetected regional biases in the observations has been underlined in several studies [e.g., *Rayner et al.*, 2002; *Patra et al.*, 2003]. *Chevallier et al.* [2005a] quantified the tolerance of the inversion systems on the basis of the statistics of the observation minus prior departures $\mathbf{d} = \mathbf{y} - \mathbf{H}\,\mathbf{x_b}$. They indicate that biases larger than about one tenth of the variation of the departures are likely to degrade the quality of the analysis increments. The upper part of Figure 4 shows the departure statistics in our simulations. On the basis of the former criterion, a few tenths of a part per million bias would be enough to affect the inversions to some extent, in particular over sea. We checked this property by introducing known biases in our simulated observations. There are several potential sources of biases in the satellite estimate of X_{CO2}, each with a particular spatial and temporal pattern. As an example, we focus here on the potential impact of submicron aerosol particles, the optical thickness of which has a strong and variable spectral signature, which could be a source of error [*O'Brien and Rayner*, 2002]. These aerosols are mostly generated by anthropogenic activities and biomass burning. For the present experiment, we used 3D aerosol concentrations derived from the assimilation of satellite retrievals of aerosol optical depths into an atmospheric transport model [*Generoso et al.*, 2007]. For this exercise, we assume a bias (in ppm) in the OCO retrievals as five times the submicronic aerosol 850 nm optical thickness (unitless). The bias is defined so that it increases the observation value. The global average bias is 0.29 ppm while the 90th percentile is 0.49 ppm. With this choice, the bias is, on average, one order of magnitude smaller than the departure standard deviation (see Figure 4, bottom). Some regions show a more significant bias however, in particular downwind of China, North America and Europe. Regions of biomass burning (Sahel, South Africa, South and Central America) also show significant biases, but only during the corresponding season so that the impact on the annual mean is small. The large values around 50°S are the result of

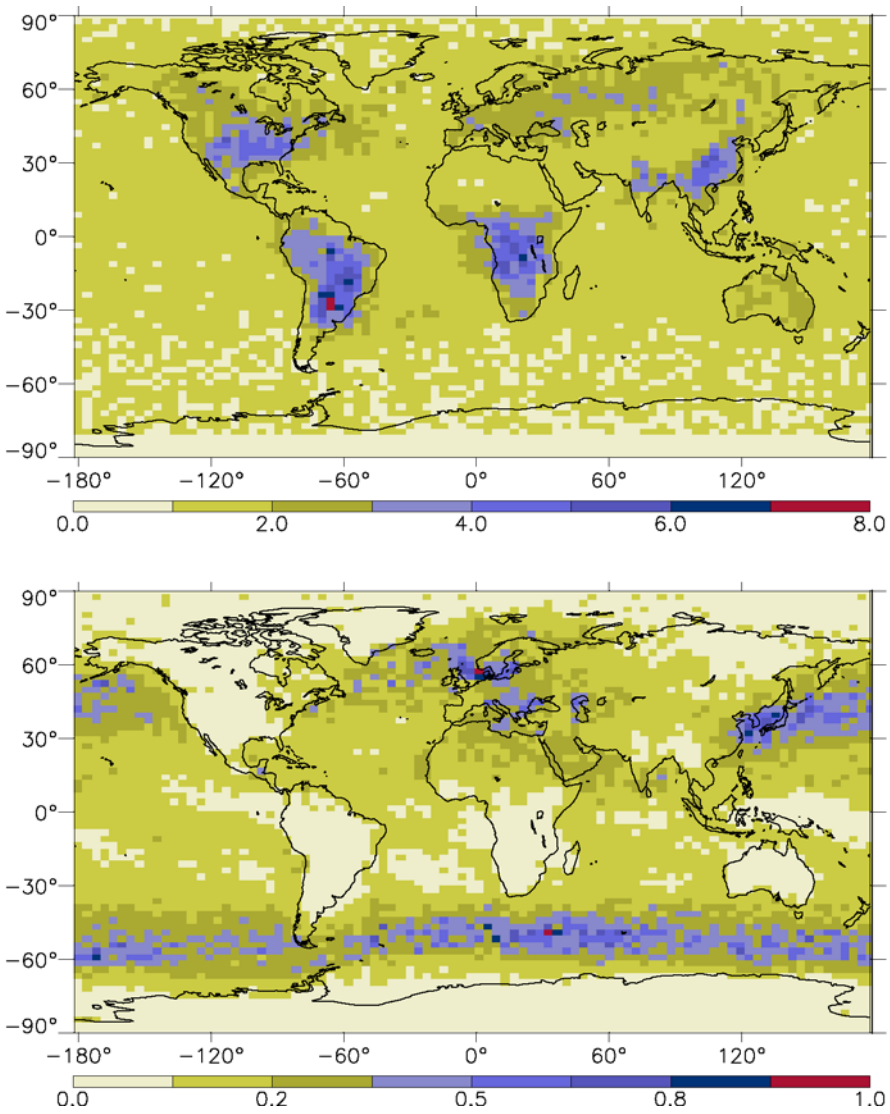

Figure 4. (top) Standard deviation (in ppm) of the observation minus prior departure. (bottom) Ratio of the annual mean bias introduced in the inversions to this standard deviation.

both marine aerosol load and small departure standard deviations.

[36] The impact of the biases on the inversion is illustrated by the resulting bias in the annual carbon budget in each one of the 22 TransCom3 regions (Figure 5). As expected, significant biases occur in Europe (0.6 Gt C yr^{-1}), in temperate Eurasia (0.7 Gt C yr^{-1}), in Northern and Southern temperate America (0.25 Gt C yr^{-1} in both cases). Over the oceans, a 0.2 Gt C yr^{-1} bias is seen in the Southern ocean. Interestingly, the inversion system generates negative flux biases to conserve CO_2 mass between the areas where the observations are biased and the ones located downstream. For instance, the boreal Eurasian region, downstream of Europe, is biased by about −0.2 Gt C yr^{-1}. By comparison, the analysis error standard deviation for monthly fluxes is between 0.1 and 0.2 Gt C yr^{-1} in each region and the prior one between 0.1 and 0.7 Gt C yr^{-1} (not shown). The biased analysis has still smaller root mean square errors (RMSE) than the prior in all land regions, but Europe and temperate Eurasia. Owing to the small prior errors over ocean, the observation bias cancels any RMSE improvement in these two regions.

4. Discussion and Conclusions

[37] The variational formulation of Bayesian estimation plays an increasingly important role for the analysis of large numbers of observations, as is the case for satellite data. It circumvents the difficulty of inverting a large and possibly dense matrix in the search for the minimum variance solution. Unfortunately, unlike the formulation by a suite of matrix operations, the characterization of the uncertainty of this solution remains a challenge, which affects the conditioning of the minimization and hampers the computation of useful diagnostics, like the number of degrees of freedom for signal or the observation influence matrix. A few strategies have been proposed to estimate some quantities related to the analysis error covariance matrix, based on randomization [*Rabier and Courtier*, 1992; *Fisher*, 2003; *Desroziers et al.*, 2005] or on reduced rank decomposition

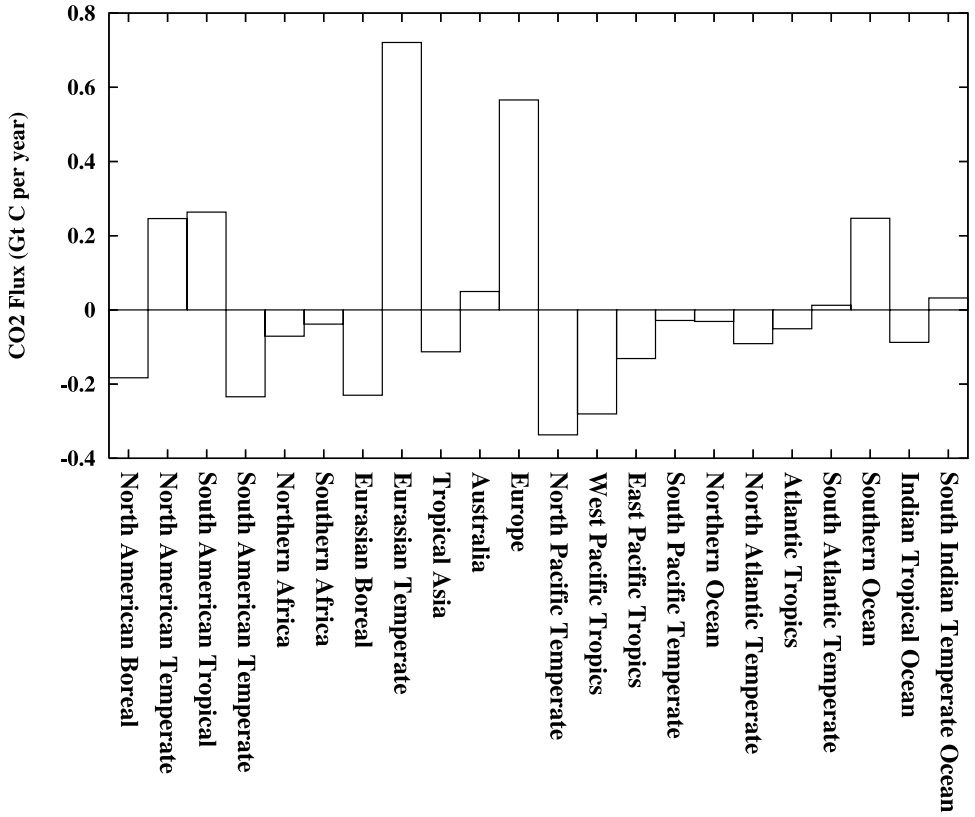

Figure 5. Flux bias (in Gt C yr^{-1}) induced by the OCO bias of Figure 4 in each one of the 22 TransCom-3 regions.

[*Fisher and Courtier*, 1995]. More directly, the influence of observations on an assimilation system is also studied by comparison to independent observations or with observing system simulation experiments (OSSE). For OSSEs, the "truth" is usually defined from another model, which is likely to be inconsistent with the specified prior errors. Our study combines an OSSE framework with a randomization approach to build OCO observations and prior fluxes that are perfectly consistent with their specified error statistics. This method relies on the availability of sufficiently accurate reduced-rank eigenvector decompositions of the prior and of the observation errors. This is straightforward for the observation error covariance matrix which is usually diagonal. The prior error covariance matrix is usually built in such a way that it has both realistic features and convenient mathematical properties [e.g., *Derber and Bouttier*, 1999], so that its eigenvalue decomposition may also be available despite its large dimension, as is the case here. Our approach allows one to directly estimate mean analysis error variances and the number of degrees of freedom for signal as by-products of the inversion. It also helps to choose the number of iterations of the minimization procedure. These possibilities may motivate the design of such OSSEs for both existing and future instruments. Additional benefit may be found for the minimization preconditioning, but this remains a topic for future work.

[38] Our method has been applied to the estimation of the impact of the forthcoming OCO observations on the analysis of CO_2 surface fluxes. Other CO_2 observations could be usefully studied in a similar way (e.g., those from NASA's Atmospheric Infra-Red Sounder or those from the forthcoming Greenhouse Gases Observing Satellite planned by the Japan Aerospace Agency). Given our assigned error statistics for the prior fluxes and the observations, we show significant error reduction even at the weekly timescale and at the grid point resolution over land (15–45% over vegetated areas). The reduction over oceans becomes significant (20–40%) only when aggregating at the oceanic basin monthly scales. These results are consistent with the results from previous low-resolution studies. They are based on a series of reasonable assumptions about the error statistics, the importance of which needs to be stressed. The error statistics are assumed to be unbiased, Gaussian, uncorrelated for the observations, uncorrelated in time and correlated with an *e*-folding distance by geotype in space. Therefore our study should be considered as a best-case estimate and careful examination of each one of these hypotheses will be essential for optimal use of the OCO data. The existence of regional biases, or equivalently of strong spatial correlations, linked to scattering by clouds and aerosols, is of particular concern. We show that the failure to limit the regional biases to within a few tenths of a part per million would have a detrimental impact on the flux estimation. Therefore the usefulness of OCO observations for the study of the carbon cycle will depend on the quality control of the data. The assimilation of OCO observations in concert with another instrument would reduce the impact of the biases provided the biases of the two observing systems do not share the same space-time characteristics. A similar issue could be raised about the biases of the transport

models that are used to link the atmospheric measurements to the boundary fluxes. It is important to stress that the exploitation of the surface network for flux inversion faces the same challenges. Other issues that still need to be addressed are the contributions of fossil fuel emissions and biomass burning, whose distinct features are not studied here, i.e., a large spatiotemporal variability and an injection height possibly well above the surface.

[39] In our reference case estimate, the uncertainty in the monthly carbon budget over Europe is reduced by 70%, leaving a residual uncertainty of about 0.16 Gt C yr^{-1} (annual total). By comparison, the 2003 European summer drought induced an anomaly of about 0.5 Gt C [*Ciais et al.*, 2005], so that such large climate induced anomaly should be detected by an observation system like OCO plus a suitable assimilation system. However, it is very unlikely that a single CO_2-sensitive satellite instrument, like OCO, will be sufficient to address scientific questions about smaller signals (like the compliance to international treaties) or smaller scales (like the quantification of the role of peatlands raised by *Sottocornola and Kiely* [2005]). For instance, European fossil emissions are less than 1 Gt C yr^{-1}, while the reduction objective of the Kyoto protocol (see http://unfccc.int/) are of a few percent averaged on a 5-year period. The verification of European compliance with the Kyoto protocol therefore requires an accuracy of the order of 1 percent of current emissions, or 0.01 Gt C yr^{-1}. Our results indicate that such accuracy is not feasible with an OCO-like instrument alone. Following the example of numerical weather prediction, a multi-instrument strategy is desirable to build robust carbon cycle data assimilation systems.

[40] **Acknowledgments.** The authors wish to thank M. Fisher (ECMWF), P. Peylin, P. Ciais (LSCE), and A. S. Denning (LSCE/CSU) for fruitful interactions; F. Delage (LSCE) for kind help with the plots; and F. Marabelle (LSCE) for computer support. D. Crisp, C. Miller (JPL), R. Engelen, A. Hollingsworth (ECMWF), and three anonymous reviewers provided useful comments on an earlier version of this article. Some of the computations were performed at the Centre de Calcul Recherche et Technologie (CCRT). The study was cofunded by the European Union under the project GEMS.

References

Andersson, E., M. Fisher, R. Munro, and A. McNally (2000), Diagnosis of background errors for radiances and other observable quantities in a variational data assimilation scheme, and the explanation of a case of poor convergence, *Q. J. R. Meteorol. Soc.*, *126*, 1455–1472.

Baker, D. F., S. C. Doney, and D. S. Schimel (2006), Variational data assimilation for atmospheric CO_2, *Tellus, Ser. B*, *58*, 359–365.

Bousquet, P., P. Peylin, P. Ciais, C. Quere, P. Friedlingstein, and P. Tans (2000), Regional changes in carbon dioxide fluxes of land and oceans since 1980, *Science*, *290*, 1342–1346.

Bréon, F. M., D. M. O'Brien, and J. D. Spinhirne (2005), Scattering layer statistics from space borne GLAS observations, *Geophys. Res. Lett.*, *32*, L22802, doi:10.1029/2005GL023825.

Chevallier, F., R. J. Engelen, and P. Peylin (2005a), The contribution of AIRS data to the estimation of CO_2 sources and sinks, *Geophys. Res. Lett.*, *32*, L23801, doi:10.1029/2005GL024229.

Chevallier, F., M. Fisher, P. Peylin, S. Serrar, P. Bousquet, F.-M. Bréon, A. Chédin, and P. Ciais (2005b), Inferring CO_2 sources and sinks from satellite observations: Method and application to TOVS data, *J. Geophys. Res.*, *110*, D24309, doi:10.1029/2005JD006390.

Chevallier, F., N. Viovy, M. Reichstein, and P. Ciais (2006), On the assignment of prior errors in Bayesian inversions of CO_2 surface fluxes, *Geophys. Res. Lett.*, *33*, L13802, doi:10.1029/2006GL026496.

Ciais, P., et al. (2005), Europe-wide reduction in primary productivity caused by the heat and drought in 2003, *Nature*, *437*, 529–533.

Courtier, P., J.-N. Thepaut, and A. Hollingworth (1994), A strategy for operational implementation of 4D-Var using an incremental approach, *Q. J. R. Meteorol. Soc.*, *120*, 1367–1387.

Crisp, D., et al. (2004), The Orbiting Carbon Observatory (OCO) mission, *Adv. Space Res.*, *34*(4), 700–709.

Derber, J. C., and F. Bouttier (1999), A reformulation of the background error covariance in the ECMWF global data assimilation system, *Tellus, Ser. A*, *51*, 195–221.

Desroziers, G., P. Brousseau, and B. Chapnik (2005), Use of randomization to diagnose the impact of observations on analyses and forecasts, *Q. J. R. Meteorol. Soc.*, *131*, 2821–2837.

Enting, I. G. (2002), *Inverse Problems in Atmospheric Constituent Transport*, Cambridge Univ. Press, New York.

Enting, I. G., C. M. Trudinger, and R. J. Francey (1995), A synthesis inversion of the concentration and $\delta^{13}C$ atmospheric CO_2, *Tellus, Ser. B*, *47*, 35–52.

Fisher, M. (1998), Minimization algorithms for variational data assimilation, in *Seminar on Recent Developments in Numerical Methods for Atmospheric Modelling, 7–11 September 1998*, pp. 364–385, Eur. Cent. for Medium-Range Weather Forecasts, Reading, U. K.

Fisher, M. (2003), Estimation of entropy reduction and degrees of freedom for signal for large variational analysis systems, *ECMWF Tech. Memo. 397*, 18 pp., Eur. Cent. for Medium-Range Weather Forecasts, Reading, U. K. (Available at http://www.ecmwf.int/publications/library/ecpublications/_pdf/tm/301-400/tm397.pdf.)

Fisher, M., and P. Courtier (1995), Estimating the covariance matrices of analysis and forecast error in variational data assimilation, *ECMWF Tech. Memo. 220*, 35 pp., Eur. Cent. for Medium-Range Weather Forecasts, Reading, U. K. (Available at http://www.ecmwf.int/publications/library/ecpublications/_pdf/tm/001-300/tm220.pdf.).

Generoso, S., F.-M. Bréon, F. Chevallier, Y. Balkanski, M. Schulz, and I. Bey (2007), Assimilation of POLDER aerosol optical thickness into the LMDz-INCA model: Implications for the Arctic aerosol burden, *J. Geophys. Res.*, *112*, D02311, doi:10.1029/2005JD006954.

Gurney, K. R., et al. (2002), Towards robust regional estimates of CO_2 sources and sinks using atmospheric transport models, *Nature*, *415*, 626–630.

Hourdin, F., and A. Armengaud (1999), Test of a hierarchy of finite-volume schemes for transport of trace species in an atmospheric general circulation model, *Mon. Weather Rev.*, *127*, 822–837.

Houweling, S., F.-M. Bréon, I. Aben, C. Rödenbeck, M. Gloor, M. Heimann, and P. Ciais (2004), Inverse modeling of CO_2 sources and sinks using satellite data: A synthetic inter-comparison of measurement techniques and their performance as a function of space and time, *Atmos. Chem. Phys.*, *4*, 523–538.

Houweling, S., W. Hartmann, I. Aben, H. Schrijver, J. Skidmore, G.-J. Roelofs, and F.-M. Bréon (2005), Evidence of systematic errors in SCIAMACHY-observed CO_2 due to aerosols, *Atmos. Chem. Phys.*, *5*, 3003–3013.

Ide, K., P. Courtier, M. Ghil, and A. C. Lorenc (1997), Unified notation for data assimilation: Operational, sequential and variational, *J. Meteorol. Soc. Jpn.*, *75*, 181–189.

Intergovernmental Panel on Climate Change (2001), *Climate Change 2001: The Scientific Basis*, edited by J. T. Houghton et al., 881 pp., Cambridge Univ. Press, New York.

Janisková, M., J.-F. Mahfouf, J.-J. Morcrette, and F. Chevallier (2002), Linearized radiation and cloud schemes in the ECMWF model: Development and evaluation, *Q. J. R. Meteorol. Soc.*, *128*, 1505–1528.

Lafont, S., L. Kergoat, G. Dedieu, A. Chevillard, E. Kjellström, U. Karstens, and O. Kolle (2002), Spatial and temporal variability of land CO_2 fluxes estimated with remote sensing and analysis data over western Eurasia, *Tellus, Ser. B*, *54*, 820–833.

Lorenc, A. C. (1988), Optimal nonlinear objective analysis, *Q. J. R. Meteorol. Soc.*, *114*, 205–240.

Ménard, R., S. E. Cohn, L.-P. Chang, L. Lang-Ping, and P. M. Lyster (2000), Assimilation of stratospheric chemical tracer observations using a Kalman filter. part I: Formulation, *Mon. Weather Rev.*, *128*, 2654–2671.

O'Brien, D. M., and P. J. Rayner (2002), Global observations of the carbon budget: 2. CO_2 column from differential absorption of reflected sunlight in the 1.61 μm band of CO_2, *J. Geophys. Res.*, *107*(D18), 4354, doi:10.1029/2001JD000617.

Olivier, J. G. J., A. F. Bouwman, C. W. M. Van der Maas, J. J. M. Berdowski, C. Veldt, J. P. J. Bloos, A. J. H. Visschedijk, P. Y. J. Zandyelt, and J. L. Haverlag (1996), Description of EDGAR version 2.0. A set of global emission inventories of greenhouse gases and ozone-depleting substances for all anthropogenic and most natural sources on a per country basis and on 1 × 1 grid, *RIVM Rep. 771060 002*, *TNO MEP Rep. R96/119*, Rijksinst. voor Volksgezondheld en Mileu, Bilthoven, Netherlands.

Pak, B. C., and M. J. Prather (2001), CO_2 source inversions using satellite observations of the upper troposphere, *Geophys. Res. Lett.*, *28*, 4571–4574.

Patra, P. K., S. Maksyutov, Y. Sasano, H. Nakajima, G. Inoue, and T. Nakazawa (2003), An evaluation of CO_2 observations with Solar Occultation FTS for Inclined-Orbit Satellite sensor for surface source inversion, *J. Geophys. Res.*, *108*(D24), 4759, doi:10.1029/2003JD003661.

Rabier, F., and P. Courtier (1992), Four-dimensional assimilation in the presence of baroclinic instability, *Q. J. R. Meteorol. Soc.*, *118*, 649–672.

Rayner, P. J., and D. M. O'Brien (2001), The utility of remotely sensed CO_2 concentration data in surface source inversions, *Geophys. Res. Lett.*, *28*, 175–178.

Rayner, P. J., R. M. Law, D. M. O'Brien, T. M. Butler, and A. C. Dilley (2002), Global observations of the carbon budget: 3. Initial assessment of the impact of satellite orbit, scan geometry, and cloud on measuring CO_2 from space, *J. Geophys. Res.*, *107*(D21), 4557, doi:10.1029/2001JD000618.

Rödenbeck, C. (2005), Estimating CO_2 sources and sinks from atmospheric mixing ratio measurements using a global inverse of atmospheric transport, *MPI-BGC Tech. Rep. 6*, Max-Planck-Inst. für Biogeochem., Jena, Germany. (Available at http://www.bgc-jena.mpg.de/mpg/websiteBiogeochemie/Publikationen/Technical_Reports/tech_report6.pdf.)

Rödenbeck, C., S. Houweling, M. Gloor, and M. Heimann (2003), CO_2 flux history 1982–2001 inferred from atmospheric data using a global inversion of atmospheric transport, *Atmos. Chem. Phys.*, *3*, 1919–1964.

Rodgers, C. D. (2000), *Inverse Methods for Atmospheric Sounding: Theory and Practice*, 238 pp., World Sci., Hackensack, N. J.

Rossow, W. B., A. W. Walker, D. E. Beuschel, and M. D. Roiter (1996), International Satellite Cloud Climatology Project (ISCCP) documentation of new cloud datasets, *Rep. WMO/TD 737*, 115 pp., World Meteorol. Organ., Geneva, Switzerland.

Sadourny, R., and K. Laval (1984), January and July performance of the LMD general circulation model, in *New Perspectives in Climate Modeling*, edited by A. L. Berger and C. Nicolis, pp. 173–197, Elsevier, New York.

Sottocornola, M., and G. Kiely (2005), An Atlantic blanket bog is a modest CO_2 sink, *Geophys. Res. Lett.*, *32*, L23804, doi:10.1029/2005GL024731.

Takahashi, T., et al. (2002), Global sea-air CO_2 flux based on climatological surface ocean $pCO2$, and seasonal biological and temperature effect, *Deep Sea Res., Part II*, *49*, 1601–1622.

Talagrand, O. (1998), A posteriori evaluation and verification of analysis and assimilation algorithms, paper presented at Workshop on Diagnosis of Data Assimilation Systems, Eur. Cent. for Medium-Range Weather Forecasts, Reading, U. K., 2–4 Nov.

Trémolet, Y. (2005), Diagnostics of linear and incremental approximations in 4D-Var, *Q. J. R. Meteorol. Soc.*, *130*, 2233–2251.

F.-M. Bréon, F. Chevallier, and P. J. Rayner, Laboratoire des Sciences du Climat et de l'Environnement, IPSL, CEA, CNRS, UVSQ, Gif-sur-Yvette F-91191, France. (frederic.chevallier@cea.fr)